

## Article

# Direct Sub-Kelvin Magnetocaloric Cooling and Correlated Paramagnetism in Double Perovskite $\text{Gd}_2\text{CuTiO}_6$

Yalu Cao <sup>1,†</sup>, Xinyang Liu <sup>1,2,†</sup>, Yonglin Wang <sup>1</sup>, Cheng Su <sup>1</sup>, Zhixing Hu <sup>1</sup>, Junsen Xiang <sup>2,\*</sup> and Wentao Jin <sup>1,\*</sup> <sup>1</sup> School of Physics, Beihang University, Beijing 100191, China<sup>2</sup> Beijing National Laboratory for Condensed Matter Physics, Institute of Physics, Chinese Academy of Sciences, Beijing 100190, China

\* Correspondence: xiangjs@iphy.ac.cn (J.X.); wtjin@buaa.edu.cn (W.J.)

† These authors contributed equally to this work.

## Abstract

Adiabatic demagnetization refrigeration (ADR) has attracted considerable attention as an effective approach to reach ultra-low temperatures required for fundamental physics and quantum technologies. Here we directly characterize the cryogenic magnetocaloric performance of the rare-earth-based double-perovskite oxide  $\text{Gd}_2\text{CuTiO}_6$  (GCTO) through quasi-adiabatic demagnetization measurements. Magnetization measurements show no long-range magnetic transition above 1.8 K and indicate dominant antiferromagnetic (AFM) interactions, consistent with an AFM ordering temperature of  $T_N \approx 1.15$  K reported previously. Notably, the isothermal magnetization  $M(H)$  at 1.8 K deviates from an ideal single-ion Brillouin response and is better described by a molecular-field correction for the Gd sublattice, suggesting correlated paramagnetism persisting above  $T_N$ . In contrast to previous studies that inferred cooling performance from thermodynamic estimates, we directly validate the achievable sub-Kelvin cooling in GCTO through quasi-adiabatic measurements. In the quasi-ADR process starting from  $T_0 \sim 2$  K, demagnetization fields of 4, 6, and 9 T yield minimum temperatures of  $T_{\min} = 761.5, 452.4,$  and  $289.2$  mK, respectively, well below  $T_N$ . After complete removal of the magnetic field, the sample temperature remains highly stable for at least several tens of minutes, demonstrating a long hold time under quasi-adiabatic conditions. Moreover, the  $T(H)$  curves reveal a characteristic field scale around  $H_c \sim 1$  T, implying a field-induced modification of the low-temperature magnetic-entropy landscape that is relevant to the cooling behavior during demagnetization. These results highlight GCTO as a promising magnetic refrigerant for sub-Kelvin ADR applications and underscore the role of correlated magnetism in optimizing cryogenic magnetocaloric performance.

**Keywords:** adiabatic demagnetization refrigeration; magnetocaloric effect; double perovskite; antiferromagnetic interactions; spin correlations



Academic Editor: Dimitrios Zografopoulos

Received: 26 January 2026

Revised: 27 February 2026

Accepted: 1 March 2026

Published: 3 March 2026

**Copyright:** © 2026 by the authors.

Licensee MDPI, Basel, Switzerland.

This article is an open access article

distributed under the terms and

conditions of the [Creative Commons](https://creativecommons.org/licenses/by/4.0/)[Attribution \(CC BY\)](https://creativecommons.org/licenses/by/4.0/) license.

## 1. Introduction

The demand for reliable ultralow-temperature environments has grown rapidly in recent years, driven by advances in quantum information science, condensed matter physics, and space technology. Although dilution refrigerators and  $^3\text{He}$  sorption coolers are well established for sub-Kelvin applications, they rely heavily on scarce  $^3\text{He}$  and typically involve complex and expensive instrumentation. These limitations have renewed interest in adiabatic demagnetization refrigeration (ADR), a cooling technique that utilizes the

magnetic entropy change associated with the magnetocaloric effect (MCE) of a magnetic material to reach low temperatures [1,2]. Owing to its simple and compact design, broad compatibility with experimental setups, and independence from gravitational constraints, ADR has emerged as a promising alternative for achieving sub-Kelvin temperatures [3–8].

The performance of ADR systems is fundamentally determined by the low-temperature thermodynamic and magnetic characteristics of the refrigerant material. Conventional hydrated paramagnetic salts widely used in ADR exhibit excellent magnetocaloric performance [3,9–12]. However, their poor thermal stability and susceptibility to dehydration significantly limit their practical applications, particularly in high-vacuum environments. Moreover, most of these salts contain relatively low densities of magnetic ions, which reduces the available magnetic entropy and consequently limits their overall cooling capacity. To address these limitations, increasing attention has been directed toward compact magnetic materials that combine robust stability with high magnetic-entropy density and strong magnetocaloric performance [13–23].

Double-perovskite oxides have been widely studied due to their flexible crystal chemistry and rich magnetic ground states arising from multiple competing exchange pathways [24–30]. In particular, rare-earth-based double perovskites have attracted increasing attention as promising low-temperature magnetocaloric materials, owing to their tunable magnetism and excellent structural stability [31–33]. These compounds typically crystallize in the general formula  $A_2BB'O_6$ , where rare-earth ions reside on the  $A$  sites and transition-metal ions occupy the  $B$  sites in ordered or disordered configurations, enabling diverse magnetic interactions and substantial magnetic-entropy changes. Numerous studies have investigated the crystal structures, magnetic properties, and magnetocaloric behaviors of various rare-earth/transition-metal cation combinations in the cryogenic temperature range [31–40]. Although these studies have demonstrated large isothermal entropy changes ( $\Delta S_M$ ) and adiabatic temperature changes ( $\Delta T_{ad}$ ) in such systems, highlighting their potential in sub-Kelvin ADR, most of them rely on indirect thermodynamic indicators ( $\Delta S_M$  and  $\Delta T_{ad}$ ) derived from magnetization or heat-capacity data, while direct experimental validation of achievable cooling performance during an actual demagnetization process remains scarce.

Among them,  $Gd_2CuTiO_6$  (GCTO) has attracted particular interest recently due to its favorable low-temperature magnetic behavior and promising magnetocaloric performance [40]. It adopts a well-defined  $B$ -site-ordered double-perovskite structure, in which the  $Gd^{3+}$  ions on the  $A$  site contribute the dominant  $4f$  magnetic moments, while the  $Cu^{2+}$   $3d$  ions on the  $B$  site also contribute appreciably to the magnetism and participate in the magnetic-exchange network. First-principles calculations and experimental characterizations further indicate that the positive  $4f$ – $3d$  exchange interactions between the Gd and Cu sublattices play a crucial role in enhancing the cryogenic MCE, leading to a magnetic-entropy change that surpasses all previously reported Gd-based double perovskites. Moreover, heat capacity measurements reveal antiferromagnetic (AFM) ordering around a relatively low temperature of  $T_N = 1.15$  K, which originates from weak AFM coupling within the Gd- $4f$  sublattice [40]. These features make GCTO a particularly attractive candidate for sub-Kelvin magnetic refrigeration and ADR applications. However, existing studies on GCTO have primarily employed indirect approaches, such as evaluating the adiabatic temperature change ( $\Delta T_{ad}$ ) and isothermal entropy change ( $\Delta S_M$ ) from magnetization and specific heat data, to assess its magnetocaloric properties. Direct experimental verification of its performance during the adiabatic demagnetization process remains absent, and performing such measurements is essential for evaluating its practical viability as an ADR refrigerant.

Motivated by these considerations, the present study places primary emphasis on direct adiabatic-demagnetization measurements of GCTO, which have been absent in previous studies. Beyond conventional characterization methods, we directly monitor the sample temperature of GCTO throughout the quasi-ADR process for the first time, enabling a reliable determination of its intrinsic temperature response under varying magnetic fields. This direct approach provides a rigorous and realistic assessment of its low-temperature magnetocaloric performance and bridges the gap between ideal thermodynamic estimates and experimentally achievable ADR cooling behavior.

## 2. Materials and Methods

High-quality polycrystalline samples of GCTO were synthesized via a conventional high-temperature solid-state reaction method. Stoichiometric amounts of  $\text{Gd}_2\text{O}_3$  (99.99%),  $\text{CuO}$  (99.9%), and  $\text{TiO}_2$  (99.9%) were mixed, thoroughly ground and pelletized. The pellets were placed in an alumina crucible and sintered in air at 1100 °C for 18 h. The sintering process was repeated several times to minimize possible impurities.

The phase purity and crystal structure of the synthesized sample were characterized by powder X-ray diffraction (XRD) measurement at room temperature, utilizing a DX-27mini Benchtop X-ray diffractometer (Dandong Haoyuan Instrument Co., Ltd., Dandong, China) with  $\text{Cu K}\alpha$  radiation ( $\lambda = 1.5406 \text{ \AA}$ ). The diffraction data were collected in the  $2\theta$  range from  $10^\circ$  to  $100^\circ$  with a step size of  $0.02^\circ$ .

DC magnetization of the sample was investigated using a Quantum Design Magnetic Property Measurement System (MPMS) (Quantum Design International, Inc., San Diego, CA, USA). Temperature-dependent magnetization  $M(T)$  was measured under an applied magnetic field of 1 T in the temperature range of 1.8–300 K in zero-field-cooling (ZFC) mode. Isothermal magnetization  $M(H)$  measurement was performed at 1.8 K under magnetic fields ranging from 0 to 7 T.

The MCE measurements were conducted by directly monitoring the temperature change of the sample during the quasi-adiabatic demagnetization process, utilizing a field-calibrated  $\text{RuO}_2$  thermometer attached to the surface of the pelletized sample. A homemade sample stage was integrated into the Quantum Design Physical Property Measurement System (PPMS) [14], on which a pellet consisting of 3 g GCTO mixed with 3 g silver powder was mounted. The silver was introduced to enhance the low-temperature thermal conductivity of the otherwise insulating GCTO, thereby ensuring good internal thermal equilibration during demagnetization. Although the presence of silver increases the total heat capacity of the composite pellet and reduces the effective magnetic-entropy density of the composite pellet per unit mass, it allows the quasi-adiabatic condition to be more reliably satisfied in the present setup. The quasi-ADR process was performed under different initial conditions, with starting temperatures  $T_0$  of approximately 2 and 4 K and initial magnetic fields  $H_0$  of 2, 4, 6, and 9 T.

## 3. Results

### 3.1. Crystal Structure

The crystal structure of GCTO is illustrated in Figure 1. GCTO was reported to crystallize in a monoclinic symmetry with space group  $P2_1/c$  [40], adopting a typical double-perovskite  $A_2BB'O_6$  structure. The  $\text{Gd}^{3+}$  ions occupy the  $A$  sites, while  $\text{Cu}^{2+}$  and  $\text{Ti}^{4+}$  cations form an ordered arrangement over the distinct  $B$  and  $B'$  sites. Figure 2 shows the room-temperature XRD pattern of the synthesized polycrystalline GCTO sample, together with the corresponding Rietveld refinement based on the monoclinic structure shown in Figure 1. No impurity-related diffraction peaks are discernible, indicating that our sample is single-phase within the detection limit of laboratory XRD. The refinement

yields satisfactory agreement factors, supporting the reliability of the adopted structural model. The refined structural parameters are summarized in Table 1. Notably, the refined lattice parameters of our GCTO sample show deviations from those reported in Ref. [40], where  $a = 5.365(3) \text{ \AA}$ ,  $b = 5.579(5) \text{ \AA}$ ,  $c = 9.923(6) \text{ \AA}$  and  $\beta = 125.49(2)^\circ$  were reported. In the present work, the lattice constants are refined to be  $a = 5.3581(2) \text{ \AA}$ ,  $b = 5.7526(2) \text{ \AA}$ ,  $c = 9.234(2) \text{ \AA}$ , and  $\beta = 125.47(2)^\circ$ . While the  $a$  and  $\beta$  values remain comparable, more pronounced differences are observed in  $b$  and  $c$ . The origin of these discrepancies is currently unclear and may be related to differences in sample preparation conditions or oxygen stoichiometry.

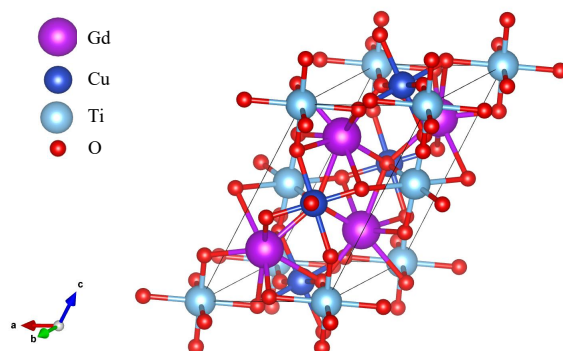


**Figure 1.** Schematic illustration of the unit cell of GCTO with a monoclinic structure, in which  $\text{Cu}^{2+}$  and  $\text{Ti}^{4+}$  ions form an ordered arrangement.

**Table 1.** Structural parameters of GCTO from Rietveld refinement to the room-temperature XRD pattern. Numbers in parentheses denote the standard uncertainties of the last significant digits obtained from Rietveld refinement.

Space Group	$P2_1/c$		
Lattice Constants	$a = 5.3581(2) \text{ \AA}$ , $b = 5.7526(2) \text{ \AA}$ , $c = 9.234(2) \text{ \AA}$ , $\beta = 125.47(2)^\circ$		
Atom (site)	$x$	$y$	$z$
Gd	0.2649(9)	0.0725(2)	0.7490(9)
Ti	0	0	0
Cu	0.5	0	0.5
O1	0.136(5)	0.036(2)	0.238(5)
O2	0.258(6)	0.676(5)	0.038(4)
O3	0.387(6)	0.194(5)	0.063(4)

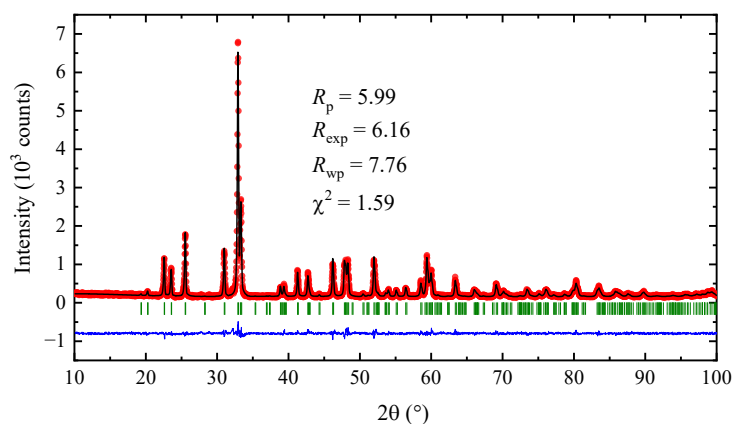


**Figure 2.** Room-temperature XRD patterns of GCTO and corresponding Rietveld refinements. The red circles represent the observed intensities, and the black solid line is the calculated pattern. The difference between the observed and calculated intensities is shown as the blue solid line at the bottom. The green vertical bars correspond to the expected Bragg reflections.

### 3.2. Magnetization Behavior

The temperature-dependent dc magnetic susceptibility  $\chi = M/H$  of GCTO, measured under an applied magnetic field of 1 T, is shown in Figure 3a.  $\chi$  increases monotonically upon cooling, and no magnetic transition is detected over the temperature range from 1.8 to 300 K, indicating typical paramagnetic behavior throughout the measured temperature interval. Curie–Weiss fit to the inverse magnetic susceptibility  $\chi^{-1}(T)$  from 10 K to 300 K yields an effective magnetic moment of  $\mu_{\text{eff}} = 11.91 \mu_{\text{B}}/\text{f.u.}$ , which is close to the theoretical value of  $\mu_{\text{eff}} = 11.36 \mu_{\text{B}}/\text{f.u.}$  expected from the free-ion moments of two  $\text{Gd}^{3+}$  ions and one  $\text{Cu}^{2+}$  ion. The slight enhancement of  $\mu_{\text{eff}}$  may be associated with the spin correlations involving the  $\text{Gd}^{3+}$  and  $\text{Cu}^{2+}$  sublattices. In addition, a negative Weiss temperature of  $\theta = -2.38 \text{ K}$  is obtained, indicating weak antiferromagnetic interactions and suggesting that the magnetic ordering temperature lies below the lowest temperature accessible in our magnetization measurements (1.8 K). Indeed, a recent heat-capacity measurement on polycrystalline GCTO has revealed an antiferromagnetic transition at  $T_{\text{N}} \approx 1.15 \text{ K}$  [40].

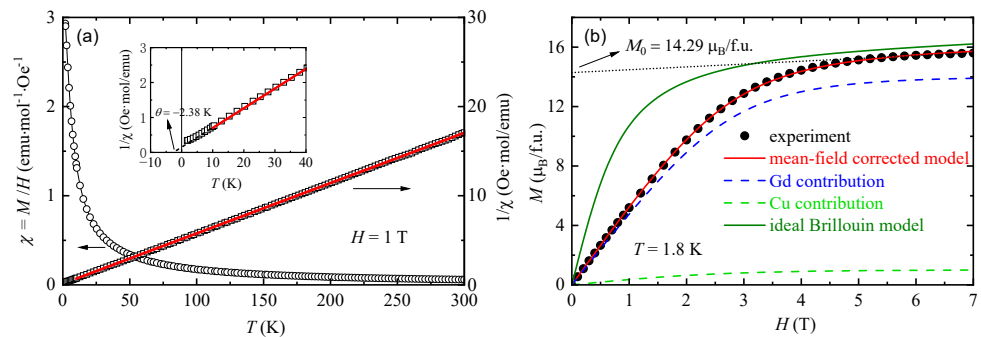


**Figure 3.** (a) DC magnetic susceptibility  $\chi = M/H$  (open circles, left axis) and inverse susceptibility  $1/\chi$  (open squares, right axis) of GCTO measured under 1 T. The red line is the Curie–Weiss fit to  $1/\chi$  from 10 to 300 K. Inset: enlarged  $1/\chi$  below 40 K, where the Curie–Weiss fit yields  $\theta = -2.38 \text{ K}$ . (b) Isothermal magnetization  $M(H)$  at 1.8 K (solid circles). The dotted line represents the high-field linear fit, whose extrapolation to  $H = 0$  gives  $M_0 \approx 14.29 \mu_{\text{B}}/\text{f.u.}$  The olive and red curves represent the ideal Brillouin model and the mean-field corrected model, respectively, with the Gd and Cu contributions shown by the blue and green dashed curves.

The isothermal magnetization  $M(H)$  measured at 1.8 K is shown in Figure 3b. The magnetization increases rapidly at low fields and gradually tends toward saturation at higher fields, consistent with a Brillouin-like response of a large-moment local-spin system. Above 5 T,  $M(H)$  increases weakly with field and reaches about  $15.60 \mu_{\text{B}}/\text{f.u.}$  at 7 T, which is significantly larger than the moment expected from two free  $\text{Gd}^{3+}$  ions ( $14 \mu_{\text{B}}/\text{f.u.}$ ). To examine this discrepancy, the high-field part of the  $M(H)$  curve was fitted with a linear function,  $M(H) = M_0 + \chi_{\text{vV}}H$ , where the linear term  $\chi_{\text{vV}}H$  accounts for the contribution from the Van Vleck paramagnetism. Extrapolating the linear fit to  $H \rightarrow 0$  yields an intercept of  $M_0 \approx 14.29 \mu_{\text{B}}/\text{f.u.}$ , which is very close to the expected saturation moment of two  $\text{Gd}^{3+}$  ions. This result indicates that the magnetization at 1.8 K is dominated by the Gd sublattice, and additional contribution from the  $\text{Cu}^{2+}$  moments is comparatively small within the experimental uncertainty.

To further validate whether the  $M(H)$  behavior at 1.8 K can be well described by an ideal paramagnetic model, the magnetization is first calculated using the Brillouin-function expression,

$$M(H, T) = 2 g_{\text{Gd}} J_{\text{Gd}} \mu_{\text{B}} B_{J_{\text{Gd}}}(x_{\text{Gd}}) + g_{\text{Cu}} S_{\text{Cu}} \mu_{\text{B}} B_{S_{\text{Cu}}}(x_{\text{Cu}}) + \chi_{\text{vV}}H, \quad (1)$$

where  $J$  or  $S$  denotes the total or spin angular-momentum quantum number,  $B$  represents the Brillouin function, and  $g$  is the Landé factor. The dimensionless parameter  $x$  is defined as  $x_{\text{Gd}} = \frac{g_{\text{Gd}} J_{\text{Gd}} \mu_{\text{B}} H}{k_{\text{B}} T}$  and  $x_{\text{Cu}} = \frac{g_{\text{Cu}} S_{\text{Cu}} \mu_{\text{B}} H}{k_{\text{B}} T}$ . The parameters in Equation (1) were fixed to  $J_{\text{Gd}} = 7/2$  and  $g_{\text{Gd}} = 2$  for  $\text{Gd}^{3+}$  (spin-only,  $L = 0$ ), and  $S_{\text{Cu}} = 1/2$  and  $g_{\text{Cu}} = 2$  for  $\text{Cu}^{2+}$  as a simplified approximation. The value of Van Vleck-like susceptibility  $\chi_{\text{VV}}$  was taken from the high-field linear fit. With no adjustable fitting parameters, the calculated curve (green solid line in Figure 3b) shows a pronounced deviation from the experimental data (black solid circles), particularly in the low-field range. This discrepancy indicates that GCTO at 1.8 K does not behave as an ideal ensemble of non-interacting paramagnetic moments. Such a deviation may be associated with spin correlations and short-range magnetic order that become non-negligible near the AFM ordering temperature, due to the proximity of 1.8 K to  $T_{\text{N}} \approx 1.15$  K [40].

To account for the deviation of the  $M(H)$  curve from the ideal single-ion Brillouin behavior at 1.8 K, a standard mean-field correction for the Gd sublattice is introduced [41–43]. In this approach, the applied field  $H$  is replaced by an effective field  $H_{\text{eff}}$  that includes an internal molecular field proportional to the magnetization,

$$H_{\text{eff}} = H + \lambda_{\text{Gd}} M_{\text{Gd}}, \quad (2)$$

where  $\lambda_{\text{Gd}}$  is an effective molecular-field coefficient that accounts for spin correlations and short-range magnetic order within the Gd sublattice in the paramagnetic state, particularly in the vicinity of  $T_{\text{N}}$ . Accordingly, the Gd contribution to the magnetization is expressed by the self-consistent equation,

$$M_{\text{Gd}}(H, T) = 2 g_{\text{Gd}} J_{\text{Gd}} \mu_{\text{B}} B_{J_{\text{Gd}}} \left[ \frac{g_{\text{Gd}} J_{\text{Gd}} \mu_{\text{B}}}{k_{\text{B}} T} (H + \lambda_{\text{Gd}} M_{\text{Gd}}) \right]. \quad (3)$$

The  $\text{Cu}^{2+}$  contribution is modeled as a spin-1/2 Brillouin response,

$$M_{\text{Cu}}(H, T) = g_{\text{Cu}} S_{\text{Cu}} \mu_{\text{B}} B_{S_{\text{Cu}}} \left( \frac{g_{\text{Cu}} S_{\text{Cu}} \mu_{\text{B}} H}{k_{\text{B}} T} \right), \quad (4)$$

while a molecular-field term is neglected for  $\text{Cu}^{2+}$  since the magnetization is dominated by the Gd sublattice and the Cu contribution is relatively small. The total magnetization is then given by

$$M(H, T) = M_{\text{Gd}}(H, T) + M_{\text{Cu}}(H, T) + \chi_{\text{VV}} H. \quad (5)$$

By fitting the experimental  $M(H)$  curve using Equation (5), the molecular-field coefficient is refined to be  $\lambda_{\text{Gd}} = -0.1422(5) \text{T} \cdot (\mu_{\text{B}}/\text{f.u.})^{-1}$ . With this mean-field correction for the Gd sublattice, the calculated curve (red solid line in Figure 3b) shows excellent agreement with the experimental data over the entire field range. The negative  $\lambda_{\text{Gd}}$  is consistent with the AFM interactions inferred from the Curie-Weiss analysis. Given that the measured saturation moment is essentially governed by the two  $\text{Gd}^{3+}$  ions, the  $\text{Cu}^{2+}$  contribution is comparatively minor. Within the experimental resolution and fitting accuracy, the influence of 4f–3d exchange at 1.8 K can be effectively incorporated into the mean-field correction applied to the dominant Gd sublattice, and introducing an additional molecular-field term for the Cu sublattice does not lead to a meaningful improvement of the fit.

### 3.3. ADR Performance

Having characterized the magnetization behavior of GCTO, we now turn to its low-temperature magnetocaloric response during the quasi-ADR process. A pronounced cooling effect of the polycrystalline GCTO sample is observed upon reducing the applied

magnetic field under quasi-adiabatic conditions. As shown in Figure 4a, the minimum temperatures achievable under different initial conditions are compared first. Starting from  $T_0 = 4$  K, demagnetization from  $H_0 = 2$  T and 4 T cools the sample down to  $T_{\min} \approx 2.5$  K and  $\approx 1.4$  K, respectively. Notably, the minimum temperatures obtained from  $T_0 = 4$  K remain substantially higher than those achieved when the demagnetization is initiated near 2 K. This is naturally expected, as the magnetic entropy is already significantly thermally populated at higher initial temperatures, which reduces the available magnetocaloric cooling efficiency during demagnetization. For measurements initiated at a lower temperature of  $T_0 \approx 2$  K (Figure 4b), demagnetization from  $H_0 = 4$  T yields  $T_{\min} = 761.5$  mK. Increasing the initial field to  $H_0 = 6$  T further reduces the minimum temperature to  $T_{\min} = 452.4$  mK. Under the highest initial field of  $H_0 = 9$  T, the sample reaches the lowest temperature of  $T_{\min} = 289.2$  mK. These results demonstrate the strong cooling capability of GCTO in the sub-Kelvin temperature range, highlighting its potential for cryogenic magnetic refrigeration.

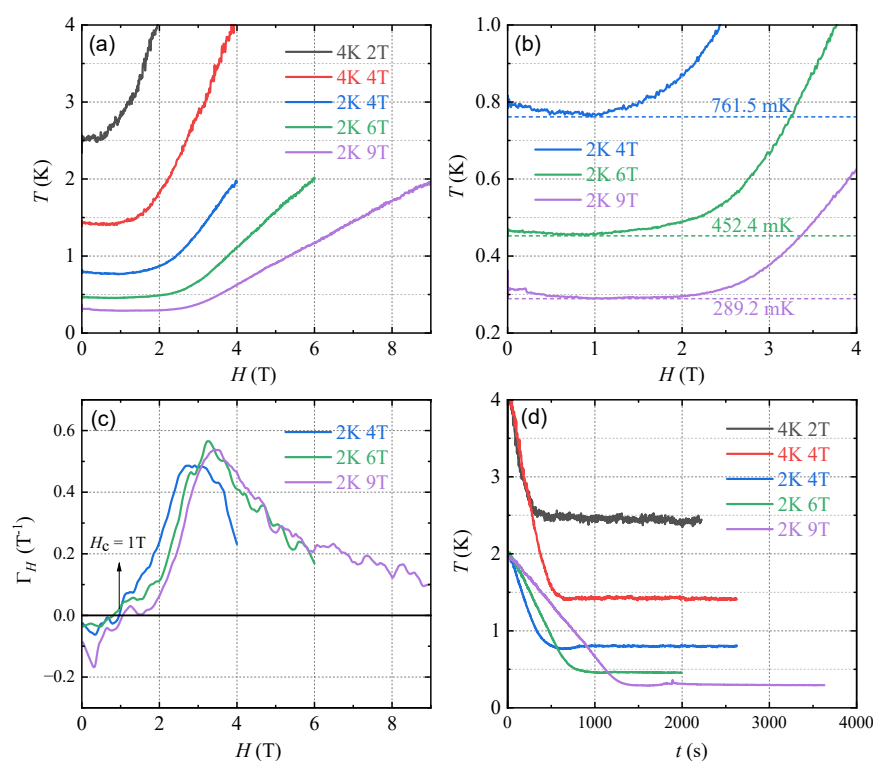


**Figure 4.** Low-temperature magnetocaloric response of GCTO measured during quasi-adiabatic demagnetization. (a) Temperature-field  $T(H)$  curves recorded under different initial conditions. (b) Enlarged low-field view of the  $T(H)$  curves initiated at  $T_0 \approx 2$  K, where the dashed lines indicate the minimum temperatures  $T_{\min}$  achieved for  $H_0 = 4, 6,$  and  $9$  T. (c) Magnetic Grüneisen parameter  $\Gamma_H = \frac{1}{T} \left( \frac{\partial T}{\partial H} \right)_S$  derived from the corresponding  $T(H)$  data, showing a sign change around  $H_c \sim 1$  T. (d) Temperature-time  $T(t)$  curves after demagnetization for the same initial conditions, showing excellent temperature stability with negligible drift after complete removal of the magnetic field.

Furthermore, the detailed temperature evolution as a function of magnetic field [ $T(H)$  curve] provides additional insight into the low-temperature magnetocaloric response of GCTO. Notably, for the demagnetization curves initiated at  $T_0 \approx 2$  K, the temperature exhibits a pronounced minimum around  $H \sim 1$  T, followed by a clear rebound upon further reducing the field, as highlighted in the enlarged low-field view in Figure 4b. Such a nonmonotonic  $T(H)$  behavior implies a strong field dependence of the magnetic entropy at low temperatures and can be characterized by the magnetic Grüneisen parameter,  $\Gamma_H = \frac{1}{T} \left( \frac{\partial T}{\partial H} \right)_S$ . As shown in Figure 4c,  $\Gamma_H$  changes sign in the vicinity of  $H_c \sim 1$  T, indi-

cating a pronounced modification of the entropy landscape as a function of field in this low-temperature regime. Although the present measurements are conducted at temperatures still above the deep quantum critical regime, the observed temperature minimum and the sign reversal of  $\Gamma_H$  together suggest a possible field-induced crossover or anomaly around  $H_c$  [44,45]. Further investigations at even lower temperatures will be helpful to clarify the nature of this anomaly around  $H_c$ .

Figure 4d presents the corresponding temperature-time ( $T$ - $t$ ) curves for different initial conditions, as recorded after the quasi-ADR process. After the magnetic field is fully removed, the sample temperature shows excellent stability with negligible drift. In particular, once the minimum temperature is reached, it can be maintained for at least tens of minutes, demonstrating a long hold time under quasi-adiabatic conditions. This behavior indicates effective thermal isolation from the environment and confirms that the demagnetization is carried out under well-controlled quasi-adiabatic conditions. The observed temperature stability further ensures that the measured  $T_{\min}$  and the adiabatic temperature changes reflect the intrinsic magnetocaloric response of GCTO, rather than being significantly affected by external heat leaks or relaxation effects. For comparison, recent reports on oxide-based quantum magnetic refrigerants such as  $\text{Na}_2\text{BaCo}(\text{PO}_4)_2$  have demonstrated holding times on the order of 1–2 h below 1 K under optimized experimental conditions [14]. We note that holding time depends sensitively on total heat capacity, thermal contact conditions, and parasitic heat leaks in the measurement setup. In the present study, the post-demagnetization evolution was monitored for approximately one hour only, during which the temperature remained stable in the sub-Kelvin regime. The current data therefore establish robust temperature stability, while not defining the absolute upper limit of the holding time.

### 3.4. Discussion

Previous heat-capacity measurements on GCTO have established its strong cryogenic magnetocaloric response through indirect thermodynamic analyses and revealed an AFM transition at  $T_N \approx 1.15$  K [40], indicating the onset of long-range magnetic ordering. In the present work, direct quasi-ADR measurements demonstrate that GCTO can be cooled well below this transition temperature, reaching minimum temperatures of 761.5, 452.4, and 289.2 mK for demagnetization fields of 4, 6, and 9 T, respectively, starting from  $T_0 \approx 2$  K. These results suggest that a substantial amount of magnetic entropy remains accessible across the magnetic ordering transition and can be effectively utilized for sub-Kelvin magnetic refrigeration.

Importantly, the isothermal magnetization at 1.8 K (Figure 3b) deviates from the ideal single-ion Brillouin response expected for a non-interacting paramagnet. A satisfactory description of the  $M(H)$  data requires the inclusion of a molecular-field correction for the Gd sublattice, with a negative molecular-field coefficient  $\lambda_{\text{Gd}}$  consistent with the Curie–Weiss analysis. Experimentally, the necessity of including such an interaction term indicates a deviation from conventional ideal paramagnetism. Meanwhile, we emphasize that magnetization data alone cannot strictly distinguish between correlated paramagnetism and short-range magnetic order in a microscopic sense, which would require complementary probes such as neutron scattering or detailed heat-capacity analysis. It is worth noting that the present magnetization data were collected at 1.8 K (above  $T_N$ ). Closer to  $T_N$ , enhanced critical spin fluctuations are expected, which may further strengthen the correlated behavior, whereas below  $T_N$  long-range AFM order dominates and the paramagnetic description is no longer applicable.

Significant spin correlations persist even above  $T_N$ , consistent with a correlated paramagnetic regime in the vicinity of the AFM transition. Such correlated paramagnetism is commonly observed in materials undergoing second-order magnetic phase transitions and

has also been reported in various magnetic refrigerants such as  $\text{Gd}_3\text{BWO}_9$  [17],  $\text{GdBO}_3$  [46], and  $\text{Na}_2\text{BaCo}(\text{PO}_4)_2$  [14], where enhanced magnetocaloric responses appear just above the ordering temperature. Microscopically, in this critical regime, the spin correlation length increases and low-energy spin fluctuations become enhanced, leading to a pronounced temperature dependence of magnetization  $\left(\frac{\partial M}{\partial T}\right)_H$ . Since the magnetic Grüneisen parameter  $\Gamma_H = \frac{1}{T} \left(\frac{\partial T}{\partial H}\right)_S$  is directly related to  $\left(\frac{\partial M}{\partial T}\right)_H$  through the Maxwell relation, these critical fluctuations can enhance the magnetocaloric response and are favorable for ADR performance. In addition, the  $T(H)$  curves measured for  $T_0 \approx 2$  K (Figure 4b) together with the derived magnetic Grüneisen parameter  $\Gamma_H$  (Figure 4c) reveal a characteristic field scale of  $H_c \sim 1$  T, where a field-induced modification of the low-temperature magnetic entropy landscape is expected. Such low-field entropy redistribution around  $H_c$  is expected to be an important factor governing the attainable minimum temperature in the ADR process [14,44–49].

Moreover, recent indirect analysis based on magnetization and heat-capacity data has predicted a significant cryogenic magnetocaloric response in GCTO [40]. In that work, both the isothermal magnetic entropy change ( $\Delta S_M$ ) and the adiabatic temperature change ( $\Delta T_{\text{ad}}$ ) were estimated from thermodynamic data. Note that  $\Delta S_M$  corresponds to an isothermal field change and therefore cannot be directly compared with the present quasi-ADR measurements, which monitor the temperature evolution  $T(H)$  of GCTO under approximately isentropic conditions. By contrast, the calculated  $\Delta T_{\text{ad}}$  provides a meaningful thermodynamic reference. From Figure 4d of Ref. [40],  $\Delta T_{\text{ad}} \approx 1.6$  K at 0.4 K for a field change of 0–5 T. Since  $\Delta T_{\text{ad}}$  represents the temperature difference between two states connected by an isentropic field variation, this implies that the thermodynamic states (0 T, 0.4 K) and (5 T, 2 K) lie approximately on the same isentropic line. Therefore, an ideal adiabatic demagnetization starting from 2 K at 5 T would reach a minimum temperature of approximately 0.4 K. However, such indirect thermodynamic estimates represent an ideal limit under perfectly isentropic conditions and do not necessarily reflect the achievable cooling performance under realistic conditions. In contrast to these thermodynamic estimates, the present work directly tracks the sample temperature during the quasi-ADR process. Starting from  $T_0 \approx 2$  K, we obtain  $T_{\text{min}} = 761.5$  mK and 452.4 mK for demagnetization fields of 4 T and 6 T, respectively. Linear interpolation yields an estimated  $T_{\text{min}} \approx 0.6$  K for 5 T, which is in reasonable agreement with the ideal thermodynamic limit of  $\sim 0.4$  K inferred above. The remaining difference can reasonably be attributed to the quasi-adiabatic character of our experiment, unavoidable heat leaks, and the additional heat capacity of the Ag powder used to improve the thermal contact.

Beyond demonstrating proximity to the ideal thermodynamic limit, our direct-ADR measurements further reveal the real cooling trajectory and the post-demagnetization hold behavior of GCTO. Our results demonstrate that GCTO can achieve a low  $T_{\text{min}}$  in the sub-Kelvin regime and maintain a long hold time of at least several tens of minutes under quasi-adiabatic conditions. These features suggest that GCTO is a promising candidate not only as a standalone cryogenic magnetic refrigerant, but also as an intermediate-stage refrigerant in multistage ADR systems. In particular, GCTO may serve as a robust oxide-based precooling stage working at relatively high magnetic fields, while conventional paramagnetic salts may be employed in the low-field regime (e.g., below  $\sim 1$  T) as a final stage to reach even lower temperatures. Such a hybrid strategy may combine the excellent thermal and chemical stability of GCTO with the superior ultra-low-temperature performance of paramagnetic salts [49–52]. The existence of a characteristic low-field entropy scale therefore may offer practical guidance for field-window optimization in ADR design.

## 4. Conclusions

In summary, we have investigated the low-temperature magnetic properties and the magnetocaloric performance of  $\text{Gd}_2\text{CuTiO}_6$  (GCTO), with a primary focus on direct quasi-adiabatic demagnetization measurements. The  $M(H)$  behavior at 1.8 K cannot be fully described by an ideal single-ion Brillouin model and instead is better captured by introducing a molecular-field correction for the Gd sublattice, indicating a correlated paramagnetic regime above the AFM ordering temperature  $T_N \approx 1.15$  K. Direct quasi-ADR measurements demonstrate that GCTO can be cooled into the sub-Kelvin range, reaching  $T_{\min} = 289.2$  mK under a demagnetization field of 9 T starting from  $T_0 \sim 2$  K, and the temperature can be stably maintained for at least several tens of minutes under quasi-adiabatic conditions. In addition, the observed low-field feature around  $H_c \sim 1$  T suggests a field-dependent modification of the low-temperature magnetic-entropy landscape, which is relevant to the cooling behavior during demagnetization. These results suggest that GCTO is a promising oxide-based magnetic refrigerant for sub-Kelvin ADR applications. We note that the present study is limited to magnetization measurements above 1.8 K and to polycrystalline samples, where magnetic anisotropy cannot be resolved. Future investigations, including low-temperature magnetization using a  $^3\text{He}$  insert, single-crystal growth to probe magnetic anisotropy, and multi-stage ADR demonstrations, will further clarify the microscopic mechanisms and optimize the refrigeration performance of GCTO. In particular, detailed studies of critical spin fluctuations and entropy redistribution near  $T_N$ , as well as systematic exploration of chemically tuned 4f–3d exchange-coupled double perovskites, may help identify a broader materials platform for cryogenic magnetic refrigeration. Such efforts may help clarify design principles linking correlated magnetism to enhanced ADR efficiency.

**Author Contributions:** Conceptualization, W.J.; Formal analysis, Y.W., C.S. and Z.H.; Methodology, Y.C., X.L., Y.W. and J.X.; Project administration, W.J.; Supervision, J.X. and W.J.; Validation, X.L. and J.X.; Visualization, Y.C.; Writing—original draft, Y.C.; Writing—review and editing, W.J. All authors have read and agreed to the published version of the manuscript.

**Funding:** This research was funded by the National Key Projects for Research and Development of China (Grant No. 2023YFA1406003), the National Natural Science Foundation of China (Grant No. 12574154, 12074024, 12404180), the Fundamental Research Funds for the Central Universities in China. This work is also supported by the Synergetic Extreme Condition User Facility (SECUF, <https://cstr.cn/31123.02.SECUF>).

**Institutional Review Board Statement:** Not applicable.

**Informed Consent Statement:** Not applicable.

**Data Availability Statement:** Data in the manuscript can be obtained by contacting the corresponding authors.

**Conflicts of Interest:** The authors declare no conflicts of interest.

## References

1. Debye, P. Einige Bemerkungen zur Magnetisierung bei tiefer Temperatur. *Ann. Der Phys.* **1926**, *386*, 1154–1160. [[CrossRef](#)]
2. Giauque, W.F. A thermodynamic treatment of certain magnetic effects. A proposed method of producing temperatures considerably below  $1^\circ$  absolute. *J. Am. Chem. Soc.* **1927**, *49*, 1864–1870. [[CrossRef](#)]
3. Giauque, W.F.; MacDougall, D.P. Attainment of Temperatures Below  $1^\circ$  Absolute by Demagnetization of  $\text{Gd}_2(\text{SO}_4)_3 \cdot 8\text{H}_2\text{O}$ . *Phys. Rev.* **1933**, *43*, 768. [[CrossRef](#)]
4. de Klerk, D. Adiabatic Demagnetization and the Temperature Scale Below  $1^\circ$  K. *Science* **1952**, *116*, 335–339. [[CrossRef](#)]
5. Gschneidner, K.A.; Pecharsky, V.K.; Tsokol, A.O. Recent developments in magnetocaloric materials. *Rep. Prog. Phys.* **2005**, *68*, 1479. [[CrossRef](#)]

6. Gutfleisch, O.; Willard, M.A.; Brück, E.; Chen, C.H.; Sankar, S.G.; Liu, J.P. Magnetic Materials and Devices for the 21st Century: Stronger, Lighter, and More Energy Efficient. *Adv. Mater.* **2011**, *23*, 821–842. [[CrossRef](#)]
7. Cao, H. Refrigeration Below 1 Kelvin. *J. Low Temp. Phys.* **2021**, *204*, 175–205. [[CrossRef](#)]
8. Koshkid'ko, Y.; Dilmieva, E.; Kamantsev, A.; Mashirov, A.; Cwik, J.; Kol'chugina, N.; Koledov, V.; Shavrov, V. Magnetocaloric Materials for Low-Temperature Magnetic Cooling. *J. Commun. Technol. Electron.* **2023**, *68*, 379–388. [[CrossRef](#)]
9. Fisher, R.A.; Hornung, E.W.; Brodale, G.E.; Giaque, W.F. Magnetothermodynamics of  $\text{Ce}_2\text{Mg}_3(\text{NO}_3)_{12} \cdot 24\text{H}_2\text{O}$ . II. The evaluation of absolute temperature and other thermodynamic properties of CMN to 0.6 m°K. *J. Chem. Phys.* **1973**, *58*, 5584–5604. [[CrossRef](#)]
10. Daniels, J.; Kurti, N. The thermal and magnetic properties of chromium potassium alum below 0.1 °K. *Proc. A* **1954**, *221*, 243–256.
11. Vilches, O.E.; Wheatley, J.C. Measurements of the Specific Heats of Three Magnetic Salts at Low Temperatures. *Phys. Rev.* **1966**, *148*, 509–516. [[CrossRef](#)]
12. Chen, Z.; Zhang, C.; Zhang, Z.; Lu, H.; Wu, L.; Zhang, G.; Tu, H.; Li, Z.; Shen, J.; Wang, D. Large cryogenic magnetocaloric effect in transition metal-based double dinitrates. *Appl. Phys. Lett.* **2024**, *125*, 262403. [[CrossRef](#)]
13. Tokiwa, Y.; Bachus, S.; Kavita, K.; Jesche, A.; Tsirlin, A.; Gegenwart, P. Frustrated magnet for adiabatic demagnetization cooling to milli-Kelvin temperatures. *Commun. Mater.* **2021**, *2*, 42. [[CrossRef](#)]
14. Xiang, J.; Zhang, C.; Gao, Y.; Schmidt, W.; Schmalzl, K.; Wang, C.W.; Li, B.; Xi, N.; Liu, X.Y.; Jin, H.; et al. Giant Magnetocaloric Effect in Spin Supersolid Candidate  $\text{Na}_2\text{BaCo}(\text{PO}_4)_2$ . *Nature* **2024**, *625*, 270–275. [[CrossRef](#)] [[PubMed](#)]
15. Liu, P.; Yuan, D.; Dong, C.; Lin, G.; Vllora, E.G.; Qi, J.; Zhao, X.; Shimamura, K.; Ma, J.; Wang, J.; et al. Ultralow-field magnetocaloric materials for compact magnetic refrigeration. *NPG Asia Mater.* **2023**, *15*, 41. [[CrossRef](#)]
16. Zhang, C.; Xiang, J.; Zhu, Q.; Wu, L.; Zhang, S.; Xu, J.; Yin, W.; Sun, P.; Li, W.; Su, G.; et al. Structural, magnetic, and magnetocaloric properties of triangular-lattice transition-metal phosphates. *Phys. Rev. Mater.* **2024**, *8*, 044409. [[CrossRef](#)]
17. Wang, Z.; Cui, X.; Treu, T.; Guo, J.; Liu, X.; Klinger, M.; Heil, C.; Ma, N.; Sheng, X.; Deng, Z.; et al. Antiferromagnetic ordering and critical behavior induced giant magnetocaloric effect in distorted kagome lattice  $\text{Gd}_3\text{BWO}_9$ . *Phys. Rev. Mater.* **2025**, *9*, 094407. [[CrossRef](#)]
18. Guo, Q.; Ren, W.; Liu, P.; Yao, J.; Xiang, J.; Zhang, K.; Wang, Y.; Kumara, L.; Wang, X.; Li, W.; et al. Giant Low-Field Magnetocaloric Effect at Sub-Kelvin Temperatures in Ferromagnetic  $\text{NH}_4\text{GdF}_4$ . *J. Am. Chem. Soc.* **2025**, *147*, 34862–34868. [[CrossRef](#)]
19. Jesche, A.; Winterhalter-Stocker, N.; Hirschberger, F.; Bellon, A.; Bachus, S.; Tokiwa, Y.; Tsirlin, A.A.; Gegenwart, P. Adiabatic demagnetization cooling well below the magnetic ordering temperature in the triangular antiferromagnet  $\text{KBaGd}(\text{BO}_3)_2$ . *Phys. Rev. B* **2023**, *107*, 104402. [[CrossRef](#)]
20. Wang, B.; Liu, X.; Hu, F.; Wang, J.; Xiang, J.; Sun, P.; Wang, J.; Sun, J.; Zhao, T.; Mo, Z.; et al. A Record-High Cryogenic Magnetocaloric Effect Discovered in  $\text{EuCl}_2$  Compound. *J. Am. Chem. Soc.* **2024**, *146*, 35016–35022. [[CrossRef](#)]
21. Arjun, U.; Ranjith, K.; Jesche, A.; Hirschberger, F.; Sarma, D.; Gegenwart, P. Efficient Adiabatic Demagnetization Refrigeration to below 50 mK with Ultrahigh-Vacuum-Compatible Ytterbium Diphosphates  $\text{AYbP}_2\text{O}_7$  ( $A=\text{Na}, \text{K}$ ). *Phys. Rev. Appl.* **2023**, *20*, 014013. [[CrossRef](#)]
22. Treu, T.; Klinger, M.; Oefele, N.; Telang, P.; Jesche, A.; Gegenwart, P. Utilizing frustration in Gd- and Yb-based oxides for milli-Kelvin adiabatic demagnetization refrigeration. *J. Phys. Condens. Matter* **2025**, *37*, 013001. [[CrossRef](#)]
23. Klinger, M.; Treu, T.; Kreisberger, F.; Heil, C.; Klinger, A.; Jesche, A.; Gegenwart, P. Sub-1 K Adiabatic Demagnetization Refrigeration with Rare-Earth Borates  $\text{Ba}_3\text{XB}_9\text{O}_{18}$  and  $\text{Ba}_3\text{XB}_3\text{O}_9$ ,  $X = (\text{Yb}, \text{Gd})$ . *Appl. Sci.* **2026**, *16*, 290. [[CrossRef](#)]
24. Vasala, S.; Karppinen, M.  $\text{A}_2\text{B}'\text{B}''\text{O}_6$  perovskites: A review. *Prog. Solid State Chem.* **2015**, *43*, 1–36. [[CrossRef](#)]
25. Hossain, A.; Bandyopadhyay, P.; Roy, S. An overview of double perovskites  $\text{A}_2\text{B}'\text{B}''\text{O}_6$  with small ions at A site: Synthesis, structure and magnetic properties. *J. Alloy. Compd.* **2018**, *740*, 414–427. [[CrossRef](#)]
26. Wu, M.X.; Li, M.R. Multiferroic properties of exotic double perovskite  $\text{A}_2\text{BB}'\text{O}_6$ . *Acta Phys. Sin.* **2018**, *67*, 157510.
27. Cook, A.M.; Paramakanti, A. Double Perovskite Heterostructures: Magnetism, Chern Bands, and Chern Insulators. *Phys. Rev. Lett.* **2014**, *113*, 077203. [[CrossRef](#)]
28. Pardo, V.; Pickett, W.E. Compensated magnetism by design in double perovskite oxides. *Phys. Rev. B* **2009**, *80*, 054415. [[CrossRef](#)]
29. Jin, W.; Chun, S.H.; Kim, J.; Casa, D.; Ruff, J.P.C.; Won, C.J.; Lee, K.D.; Hur, N.; Kim, Y.J. Magnetic excitations in the double-perovskite iridates  $\text{La}_2\text{MIR}_2\text{O}_6$  ( $M = \text{Co}, \text{Ni}, \text{and Zn}$ ) mediated by  $3d-5d$  hybridization. *Phys. Rev. B* **2022**, *105*, 054419. [[CrossRef](#)]
30. Su, C.; Zeng, X.T.; Sun, K.; Sheptyakov, D.; Chen, Z.; Sheng, X.L.; Li, H.; Jin, W. Type-II antiferromagnetic ordering in the double perovskite oxide  $\text{Sr}_2\text{NiWO}_6$ . *Phys. Rev. B* **2023**, *108*, 054416. [[CrossRef](#)]
31. Li, L.; Yan, M. Recent progress in the development of  $\text{RE}_2\text{TMTM}'\text{O}_6$  double perovskite oxides for cryogenic magnetic refrigeration. *J. Mater. Sci. Technol.* **2023**, *136*, 1–12. [[CrossRef](#)]
32. Meenakshi.; Saini, S.; Panwar, N.; Ramovatar; Kumar, S. Giant magnetocaloric properties of Gd-based double perovskite compounds in cryogenic temperature range. *J. Magn. Magn. Mater.* **2025**, *614*, 172766. [[CrossRef](#)]
33. Chen, X.; Xu, J.; Xu, Y.; Luo, F.; Du, Y. Rare earth double perovskites: A fertile soil in the field of perovskite oxides. *Inorg. Chem. Front.* **2019**, *6*, 2226–2238. [[CrossRef](#)]

34. Kumar, N.; Kaushik, S.D.; Rao, K.S.; Babu, P.D.; Deshpande, S.K.; Achary, S.N.; Errandonea, D. Temperature Dependent Crystal Structure of  $\text{Nd}_2\text{CuTiO}_6$ : An In Situ Low Temperature Powder Neutron Diffraction Study. *Crystals* **2023**, *13*, 503. [CrossRef]
35. Murthy, J.K.; Chandrasekhar, K.D.; Mahana, S.; Topwal, D.; Venimadhav, A. Giant magnetocaloric effect in  $\text{Gd}_2\text{NiMnO}_6$  and  $\text{Gd}_2\text{CoMnO}_6$  ferromagnetic insulators. *J. Phys. D Appl. Phys.* **2015**, *48*, 355001. [CrossRef]
36. Jia, Y.; Wang, Q.; Qi, Y.; Li, L. Multiple magnetic phase transitions and magnetocaloric effect in double perovskites  $\text{R}_2\text{NiMnO}_6$  ( $\text{R} = \text{Dy}, \text{Ho}, \text{and Er}$ ). *J. Alloy. Compd.* **2017**, *726*, 1132–1137. [CrossRef]
37. Zhang, Y.; Zhang, B.; Li, S.; Zhu, J.; Wu, B.; Wang, J.; Ren, Z. Cryogenic magnetic properties and magnetocaloric effects (MCE) in B-site disordered  $\text{RE}_2\text{CuMnO}_6$  ( $\text{RE} = \text{Gd}, \text{Dy}, \text{Ho}$  and  $\text{Er}$ ) double perovskites (DP) compounds. *Ceram. Int.* **2021**, *47*, 18205–18212. [CrossRef]
38. Zhang, Y.; Tian, Y.; Zhang, Z.; Jia, Y.; Zhang, B.; Jiang, M.; Wang, J.; Ren, Z. Magnetic properties and giant cryogenic magnetocaloric effect in B-site ordered antiferromagnetic  $\text{Gd}_2\text{MgTiO}_6$  double perovskite oxide. *Acta Mater.* **2022**, *226*, 117669. [CrossRef]
39. Hati, A.; Mukherjee, S.; Mondal, N.; Bhowmik, S.; Manna, G.; Majumdar, S.; Giri, S. Multiferroic order and large magnetic refrigeration capacity in  $\text{Gd}_2\text{MnFeO}_6$ : Significance of magnetic frustration and Jahn-Teller distortion. *Phys. Rev. B* **2023**, *108*, 144431. [CrossRef]
40. Zhang, Y.; Na, Y.; Hao, W.; Gottschall, T.; Li, L. Enhanced Cryogenic Magnetocaloric Effect from  $4F-3d$  Exchange Interaction B-Site Ordered  $\text{Gd}_2\text{CuTiO}_6$  Double Perovskite Oxide. *Adv. Funct. Mater.* **2024**, *34*, 2409061. [CrossRef]
41. Kittel, C. *Introduction to Solid State Physics*, 8th ed.; John Wiley & Sons: New York, NY, USA, 2005.
42. Coey, J.M.D. *Magnetism and Magnetic Materials*; Cambridge University Press: Cambridge, UK, 2010.
43. Gross, M.J.; Su, T.; Bauer, J.J.; Ross, C.A. Molecular-field-coefficient modeling of temperature-dependent ferrimagnetism in a complex oxide. *Phys. Rev. Appl.* **2024**, *21*, 014060. [CrossRef]
44. Zhu, L.; Garst, M.; Rosch, A.; Si, Q. Universally Diverging Grüneisen Parameter and the Magnetocaloric Effect Close to Quantum Critical Points. *Phys. Rev. Lett.* **2003**, *91*, 066404. [CrossRef] [PubMed]
45. Garst, M.; Rosch, A. Sign change of the Grüneisen parameter and magnetocaloric effect near quantum critical points. *Phys. Rev. B* **2005**, *72*, 205129. [CrossRef]
46. Lin, W.; Zhao, N.; Li, Z.; An, W.; Guo, R.; Wang, J.; Pan, C.; Wen, B.; Sheng, J.; Wu, L.; et al. Quantum Fluctuation-enhanced Milli-Kelvin Magnetic Refrigeration in Triangular Lattice Magnet  $\text{GdBO}_3$ . *arXiv* **2025**, arXiv:2504.08636. [CrossRef]
47. Wolf, B.; Tsui, Y.; Jaiswal-Nagar, D.; Tutsch, U.; Honecker, A.; Remović-Langer, K.; Hofmann, G.; Prokofiev, A.; Assmus, W.; Donath, G.; et al. Magnetocaloric effect and magnetic cooling near a field-induced quantum-critical point. *Proc. Natl. Acad. Sci. USA* **2011**, *108*, 6862–6866. [CrossRef]
48. Liu, T.; Liu, X.Y.; Gao, Y.; Jin, H.; He, J.; Sheng, X.L.; Jin, W.; Chen, Z.; Li, W. Significant inverse magnetocaloric effect induced by quantum criticality. *Phys. Rev. Res.* **2021**, *3*, 033094. [CrossRef]
49. Liu, X.Y.; Gao, Y.; Li, H.; Jin, W.; Xiang, J.; Jin, H.; Chen, Z.; Li, W.; Su, G. Quantum Spin Liquid Candidate as Superior Refrigerant in Cascade Demagnetization Cooling. *Commun. Phys.* **2022**, *5*, 233. [CrossRef]
50. Shirron, P.J.; Canavan, E.R.; DiPirro, M.J.; Tuttle, J.G.; Yeager, C.J. A Multi-Stage Continuous-Duty Adiabatic Demagnetization Refrigerator. In *Advances in Cryogenic Engineering*; Shu, Q.S., Ed.; Springer: Boston, MA, USA, 2000; pp. 1629–1638.
51. Shirron, P.J. Applications of the magnetocaloric effect in single-stage, multi-stage and continuous adiabatic demagnetization refrigerators. *Cryogenics* **2014**, *62*, 130–139. [CrossRef]
52. Ke, L.; Ya-Nan, W.; Ping, L.; Fang-Qiu, Y.; Wei, D.; Jun, S. Experimental research on a 50 mK multi-stage adiabatic demagnetization refrigerator. *Acta Phys. Sin.* **2023**, *72*, 190702–1–190702–8.

**Disclaimer/Publisher's Note:** The statements, opinions and data contained in all publications are solely those of the individual author(s) and contributor(s) and not of MDPI and/or the editor(s). MDPI and/or the editor(s) disclaim responsibility for any injury to people or property resulting from any ideas, methods, instructions or products referred to in the content.